European Rotorcraft Forum

COMPREHENSIVE MIXED-SENSITIVITY $\mathscr{H}_\infty$ ON-BLADE CONTROL FOR VIBRATION REDUCTION OF THE EC-145 ROTOR

Mr Jahaz Alotaibi
jhsa1@le.ac.uk, School of Engineering, University of Leicester, Leicester, UK, LE1 7RH
Dr Rafael Morales-Viviescas
rmm23@le.ac.uk, School of Engineering, University of Leicester, Leicester, UK, LE1 7RH

Abstract
In this work, we further investigate the use of $\mathscr{H}_\infty$ control design for On-Blade Control (OBC). Mixed-Sensitivity $\mathscr{H}_\infty$ is an advanced control method developed when reliable Linear-Time-Invariant representations exist and is especially suited for multivariable control problems. The method allows the designer to specify robustness and performance demands and existing optimisation algorithms would provide a controller which optimises over such design objectives. Alotaibi and Morales recently applied the methods to an analytical and validated model available for the EC-145 helicopter. Their work showed that the method is successful in reducing significantly all 4/rev hub loads while controlling directly the rotor thrust only. In this work, we extend this approach to control directly the remaining 4/rev components of the rotor hub loads. This comprehensive approach is compared to the simpler case (thrust control only) and we outweigh benefits and disadvantages. A key outcome from this work is that the performance can be improved by pursuing the comprehensive approach, achieving a further 21% vibration reduction in average across the flight envelope. However the comprehensive approach requires further implementation requirements, such as additional sensors and increased computational power, and more controller parameters to tune which can limit its applications. Both schemes provide the benefit of having a single controller operating over the wide flight envelope, ensuring higher reliability in terms of robustness properties without the performance being too compromised.

1. INTRODUCTION

On Blade Control (OBC)[11] methods embed actuators in the main rotor blade of conventional rotorcraft in order to improve rotor performance in terms of vibration and noise, mainly. Vibration is still a paramount design consideration on conventional rotorcraft, and for this reason several OBC technologies are currently being researched and developed[6] by academia and leading rotorcraft manufacturers. The most mature OBC actuator is Active Trailing Edge Flaps (ATEF) with dual configurations, with the mechanisms mounted typically on the inboard and outboard sections of the blade for increased control authority. Key benefits of ATEF mechanisms are their conceptual simplicity and low power requirements. On the other hand, the installation of OBC mechanisms is more challenging by being located in the rotating part of the rotor, and also, their operating environment is more demanding due to the the constant and significant presence of centrifugal and Coriolis forces.

Control algorithms for OBC are developed based on the Higher Harmonic Control (HHC) concept[7]. For OBC vibration reduction applications, the main idea is to control only key harmonic coefficients of the rotor hub forces and moments by harmonic manipulation of the OBC actuators. The control algorithms are constructed on the minimisation of a performance or cost function which incorporates vibration energy levels and control efforts[8]. HHC algorithms are based on the assumption that the behaviour between the harmonic coefficients is linear but static. Therefore this approach targets steady-state performance behaviour primarily. Despite the simplifying assumptions on the rotor vibration behaviour, HHC-based algorithms work well in practice offering significant improvement in key aspects of the rotor vibration signature. However, due to the neglect of information on the open-loop dynamics,

Figure 1: EC-145 with active trailing edge flaps

useful stability robustness measures and convergence limitations might be difficult to obtain. These aspects are particularly important in practical scenarios where the rotor behaviour is subject to variations in the operating condition and high reliability is of greatest importance.

In this work we pursue a different approach to the standard HHC-based control design methods and follow instead an advanced feedback control strategy. $\mathscr{H}_\infty$ fits well for OBC control applications because of the multivariable nature of the vibration reduction problem (simultaneous reduction in multiple force and moment rotor hub components is desired). According to the authors' knowledge, this control strategy has been deployed less than a handful of times to OBC applications for helicopters with active trailing edge flaps[5,2]. In addition, the rotor vibration behaviour for hover and cruise conditions can be captured very well by Linear-Time-Invariant (LTI) representations. Unlike standard HHC-based methods, $\mathscr{H}_\infty$ methods can provide more accurate measures to estimate robustness margins which takes into account open-loop dynamics. In addition, there is more transparency in obtaining a controller that achieves a desired trade-off between robustness and performance requirements in terms of convergence rates, steady-state vibration reduction levels and control efforts. Disadvantages of $\mathscr{H}_\infty$ methods is the requirement of advanced mathematical concepts and that the obtained controllers might result being high-order, which implies additional processing power and memory requirements, although this could be addressed by the application of order-reduction methods[12].

To demonstrate the feasibility and the potential of $\mathscr{H}_\infty$ methods for OBC, Alotaibi and Morales[2] applied the method for the analytical and validated model of the EC-145 rotor embedded with a single ATEF on each blade. The model was developed by Maurice and coworkers[10,1], see Figure 1. Alotaibi and Morales' approach demonstrated that the mixed-sensitivity $\mathscr{H}_\infty$ method performed very well at a sample of cruise conditions between hover and 100 kt. The control strategy targeted 4/rev thrust coefficients by manipulation of the ATEF operating at 4/rev. Further assessment in this strategy showed that the remaining 4/rev hub load components were also reduced despite not being controlled directly. For this reason it is expected that a more comprehensive approach which controls directly all 4/rev hub components would offer improved vibration reduction metrics. Simulation results indeed corroborate this and we proceed in this work to quantify such benefits and outweigh any disadvantages against the simpler approach of just controlling the 4/rev thrust components.

The manuscript is structured into three sections: Section 2 provides a brief overview of the analytical model of the EC-145 rotor with ATEF. Section 3 provides the linearisation results required to obtain LTI models of the rotor operating at hover, 20, 40, 60, 80 and 100 kt cruise speeds. Section 4 describes the controller design strategy of the comprehensive approach, together with robustness and performance results. Section 5 provides a comparison between both control approaches and the manuscript concludes with some final remarks in Section 6.

2. EC-145 ROTOR MODEL

We provide a brief description on the implementation of the analytical model of the EC-145 main rotor to perform the control design task. The model is implemented using the main equations described in the paper of Maurice et al[10]. The model was built in MATLAB and Simulink software. The model is constructed by approximating each hingeless flexible blade as a rigid blade with equivalent hinge offsets, stiffness and dampers[8]. The model has been validated against the more comprehensive CAMRAD II (Comprehensive Analytical Model of Rotorcraft Aerodynamics and Dynamics) model and flight campaign data. The model is comprised of two major parts, a single-blade model block and the integration of the individual blade contributions to form a four-blade rotor model trimmed for forward flight conditions between 0 and 100 kt. For more details on the model, such as rotor parameter values and notation, please refer to the work by Alotaibi and Morales[1] and Maurice et al[10].

2.1. Single Blade Model

The single blade model block is comprised of two major components: single-blade dynamics and aerodynamics, see Fig. 2. Each of these blocks is explained in more detail below.

Single-Blade Dynamics: The standard three degrees-of-freedom coordinates to describe the behaviour of a single blade in the main rotor are out-

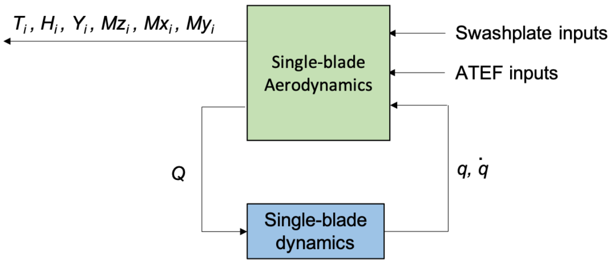

Figure 2: Overall structure of the single blade model

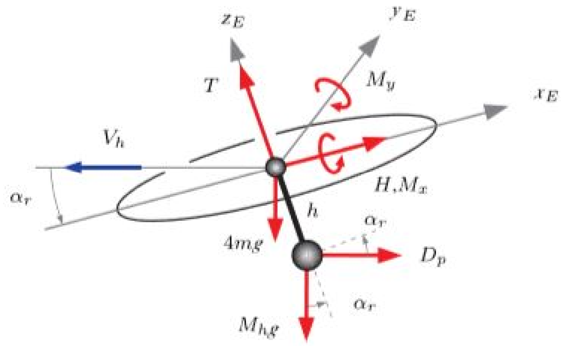

Figure 3: Forces and moments acting on the rotor hub. Picture taken from[10].

of-plane flapping β, in-plane lagging ζ, and torsional angle θ. The blade coordinates are collected in the vector

$$q = [\zeta, \beta, \theta]^T$$

with $\dot{q}$ representing dq/dt. The blade dynamics part is described by three second-order nonlinear differential equations which provide the behaviour for an individual blade given three generalized forces. The dynamic equations of motion are derived via the Lagrange method[10].

Single-Blade Aerodynamics: The aerodynamic part is constructed by solving the equations for the vector of generalized forces acting on a single blade. The generalised forces are obtained by the integration of blade-element aerodynamic forces along the radial direction and the application of the principle of virtual work[10].

$$\begin{aligned} Q &= \begin{bmatrix} Q_{lag} \\ Q_{flap} \\ Q_{pitch} \end{bmatrix} \\ &\simeq \int_{e_{air}}^{R} \begin{bmatrix} -(r-e_\zeta)dF_x + x_{aero}dF_r \\ (r-e_\beta)dF_z + x_{aero}(\Theta dF_r + \zeta dF_z) \\ dM_\Theta - x_{aero}(dF_z + \Theta dF_x) \end{bmatrix} dr \end{aligned}$$

The integration of the generalized forces has been implemented analytically to increase the computational efficiency and the accuracy of the model[1].

2.2. Blade Forces and Moments

Assuming identical blades, the rotating blade forces and moments are integrated along the span to provide the net aerodynamic forces and moments produced by each single blade. The parameter $i = 1,\dots,N$ is used as the blade index, where the number of blades in this case is $N = 4$. The blade's contributions to the rotor's vertical force, drag force, side force, torque around the vertical, pitch and roll moments are denoted in this work by $T_i, H_i, Y_i, Mz_i, My_i$ and Mx_i, respectively, and their expressions are provided below:

$$T_i = \int_{e_{air}}^{R} dFz_i dr$$

$$H_i = \int_{e_{air}}^{R} (dFx_i \sin(\psi_i) + dFr_i \cos(\psi_i))dr$$

$$Y_i = \int_{e_{air}}^{R} (-dFx_i \cos(\psi_i) + dFr_i \sin(\psi_i))dr$$

$$Mz_i = \int_{e_{air}}^{R} r\, dFx_i\, dr$$

$$My_i = \int_{e_{air}}^{R} r\, \cos(\psi_i)\, dFz_i\, dr$$

$$Mx_i = \int_{e_{air}}^{R} r\, \sin(\psi_i) dFz_i\, dr$$

2.3. Hub Loads

The rotor thrust T is normal to the blade disk, the net drag force H and net side force Y are in the disk plane, see Figure 3. In addition, there is a torque moment Mz around the shaft, positive for a rotor absorbing power. The net rotor pitch and roll moments are My and Mx, respectively. These hub forces and moments are obtained by summing over all the blades' forces and moments

$$T(t) = \sum_i^N T_i(t) \qquad H(t) = \sum_i^N H_i(t)$$

$$Y(t) = \sum_i^N Y_i(t) \qquad Mz(t) = \sum_i^N Mz_i(t)$$

$$My(t) = \sum_i^N My_i(t) \qquad Mx(t) = \sum_i^N Mx_i(t)$$

3. LINEARISATION

In line with rotor vibration theory[8], the vibration signature of the EC-145 analytical model is dominated by the blade passage frequency 4/rev in cruise flight conditions[9]. With the purpose to capture the vibration behaviour for all hub load coefficients as a LTI system, the ATEF mechanism is restricted to operate at 4/rev

$$\eta(t) = \eta_c(t)\cos(4\psi) + \eta_s(t)\sin(4\psi)$$

where ψ is the azimuth position in radians of the reference blade. $\eta(t)$ denotes the flap deflection angles in radians on the reference blade and the flap signal is shifted in the subsequent blades according to their azimuth angle.

In steady-state operating conditions and for sufficiently small ATEF deflection amplitudes, the 4/rev ATEF deflections would yield hub loads dominated also by a 4/rev harmonic plus a bias term

$$\begin{aligned}
T(t) &\approx T_{4c}(t)\cos(4\psi) + T_{4s}(t)\sin(4\psi) + T_o \\
H(t) &\approx H_{4c}(t)\cos(4\psi) + H_{4s}(t)\sin(4\psi) + H_o \\
Y(t) &\approx Y_{4c}(t)\cos(4\psi) + Y_{4s}(t)\sin(4\psi) + Y_o \\
Mz(t) &\approx Mz_{4c}(t)\cos(4\psi) + Mz_{4s}(t)\sin(4\psi) + Mz_o \\
My(t) &\approx My_{4c}(t)\cos(4\psi) + My_{4s}(t)\sin(4\psi) + My_o \\
Mx(t) &\approx Mx_{4c}(t)\cos(4\psi) + Mx_{4s}(t)\sin(4\psi) + Mx_o
\end{aligned}$$

The signals that are targeted here by the OBC vibration reduction system are the 4/rev coefficients, while the bias term is regulated for flight control purposes instead. Therefore, from the vibration controller point of view , the control inputs become

$$u(t) = [\eta_{4c}(t), \eta_{4s}(t)]^T$$

and the outputs are

$$\begin{aligned}
y(t) = [&T_{4c}(t), T_{4s}(t), H_{4c}(t), \ldots \\
&H_{4s}(t), Y_{4c}(t), Y_{4s}(t), \ldots \\
&Mz_{4c}(t), Mz_{4s}(t), My_{4c}(t), \ldots \\
&My_{4s}(t), Mx_{4c}(t), Mx_{4s}(t)]^T
\end{aligned}$$

The linearity assumption (4/rev inputs leads to 4/rev outputs) forms the foundation of the identification process and enables the successful implementation of $\mathscr{H}_\infty$ control design methods. We approximate the vibration behaviour in the Laplace domain as

$$(1) \quad y(s) = G(s)\eta(s) + d(s)$$

See Figure 4. $y(s)$ and $\eta(s)$ represent the Laplace transform of $y(t)$ and $\eta(t)$, respectively. $d(s)$ is the Laplace transform of the baseline vibration

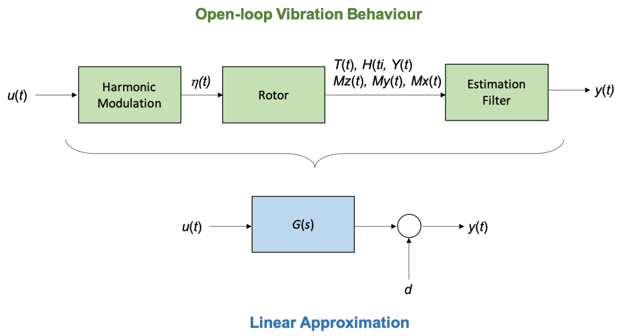

Figure 4: Open-loop Vibration Behaviour and Linear Approximation.

$$d = [T_o, H_o, Y_o, Mz_o, My_o, Mx_o]^T$$

which can be measured in the presence of zero flapping. The goal of the system identification task in this section is to represent the unbiased vibration behaviour by a transfer function matrix $G(s)$ (of size 12 by 2), providing a very good approximation between the system represented by (1) and the vibration obtained by the EC-145 rotor model implemented by Alotaibi and Morales[1]. Note that in practical implementations, the control approach would require two signal processing elements, denoted as the Harmonic Modulation and the Estimation Filter. While the former is required to ensure that ATEF deflections are restricted to operate at 4/rev only, the latter is required to estimate the 4/rev harmonic coefficients for all hub loads.

3.1. Linearisation Results

Initial experiments in open loop corroborated that 4/rev ATEF components were largely decoupled from the bias terms in the hub loads. This is particularly beneficial because such inputs are desired not to interfere with the trimming of the rotor or the flight control mechanism. The linearisation was performed using Matlab's System Identification toolbox to extract two-input twelve-output Linear-Time-Invariant models in cruise conditions at hover, 20, 40, 60, 80 and 100 kt. Such linear approximations are obtained after the rotor is trimmed with zero trailing edge flapping.

In the process of model linearisation, we increase the order of the transfer function until we have a very good matching between the linear and nonlinear responses for the same ATEF input signals. Increasing too much the order for better identification results would lead to high-order controllers. In the end, each transfer function element was cho-

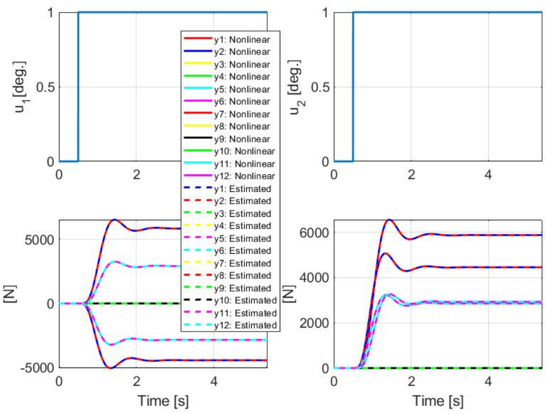

Figure 5: Linearization results for hover.

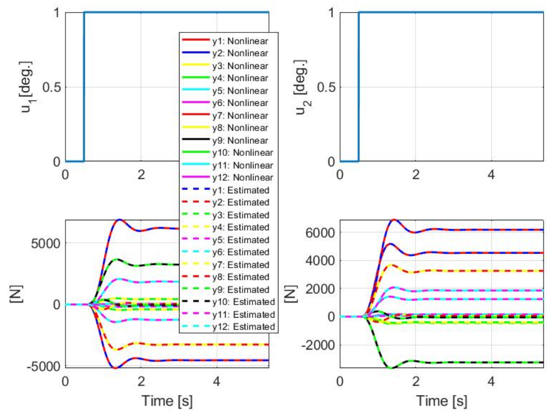

Figure 6: Linearization results at 20 knots.

sen as a third order, see Figures 5 - 10. The inputs in these graphs denoted as u_1 and u_2 correspond to η_{4c} and η_{4s}, respectively. Similarly, the output shown as y_k correspond to the k-th element of the vector signal $y(t)$. Each of the elements of the transfer function was obtained using the system identification function tfest. Step signals as shown in each of the graphs were applied and the responses were recorded. This process was repeated for each input separately. As shown in the results for all conditions, the match provided by the system ID tool was considered very good, with the responses from the transfer function matrix being almost identical in most cases to those provided by the nonlinear analytical model. The overall behaviour of the six identified linear systems characterised in the frequency domain can be observed in Figure 11. In this figure, we read two singular values associated with the largest and minimum gains of the system. Clearly, the behaviour of the system varies noticeably across cruise speeds. The system exhibits very large gain for frequencies up to the bandwidth region of about 10 rad/s, which is good news in terms of control authority. No light damping is observed in all flight conditions, which again facilitates the control design task.

4. CONTROL DESIGN AND SIMULATION RESULTS

In this section, a $\mathscr{H}_\infty$ controller is designed for the linearised models. The aim of the control design is to reduce vibration reduction of EC-145 active rotor model with ATEFs. The comprehensive controller takes into account all 4/rev hub load components. Our approach to attenuate helicopter vibration is to design $\mathscr{H}_\infty$ controllers using mixed-sensitivity methods[12]. The conventional feedback interconnection

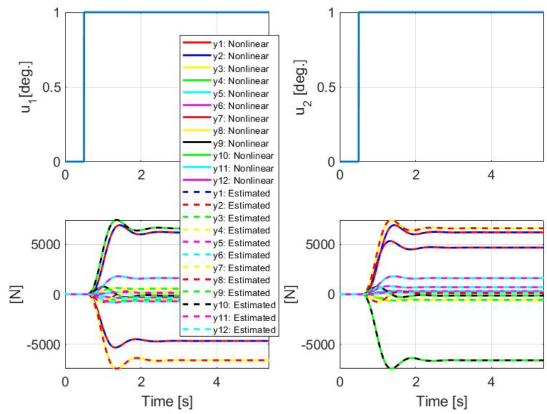

Figure 7: Linearization results at 40 knots.

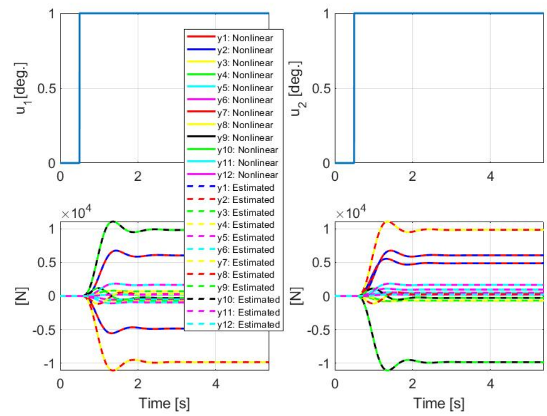

Figure 8: Linearization results at 60 knots.

is shown in Figure 12, whereby the controller $K(s)$ is the designed LTI element to attenuate rotor vibrations and the plant G represent the rotor behaviour. The control signals are denoted by $u(t)$, which in our case refer to the 4/rev components of the ATEF deflection angles. The reference signal is denoted by

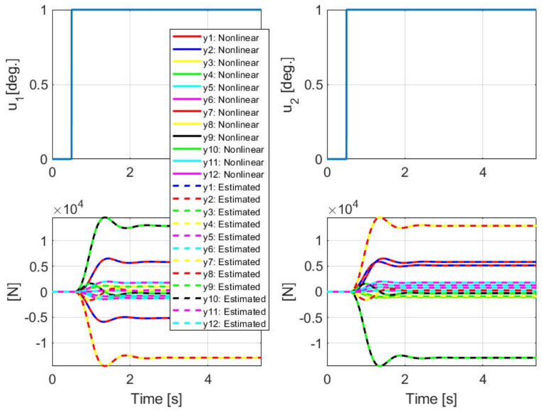

Figure 9: Linearization results at 80 knots.

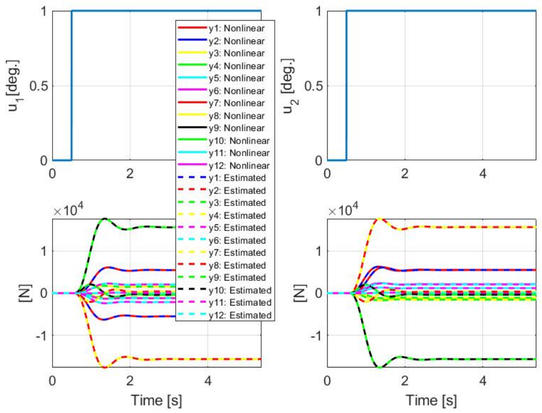

Figure 10: Linearization results at 100 knots.

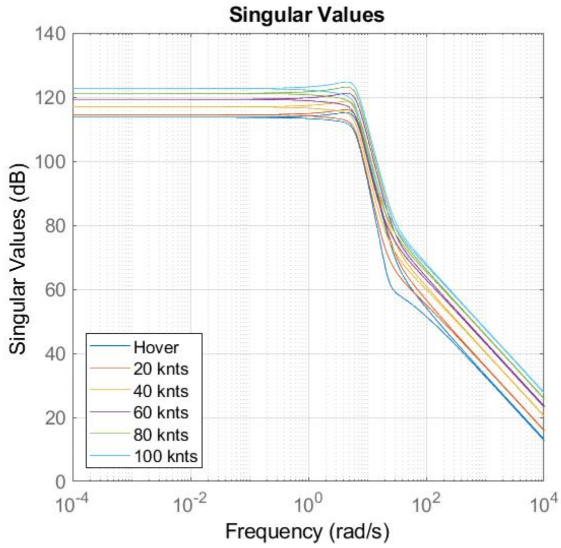

Figure 11: Frequency responses for all identified models

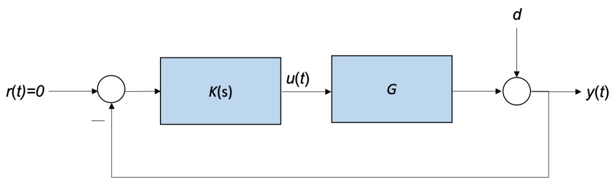

Figure 12: Classical feedback configuration

$r(t)$, which in this case is set to zero as these are the target values for the vibration outputs after closing the loop. The controller is designed first based on the models obtained from the linearisation section. Once a controller which provides satisfactory level of robustness and performance under linear simulations is obtained, then it is implemented on the nonlinear analytical model for an assessment of the performance. Typically the controller is required to be finely retuned after this to achieve improved results with the analytical rotor model.

The controller is designed to achieve the smallest peak sensitivity. The efforts were concentrated in finding a unique controller which is able to provide vibration reduction for all flight conditions. This is also desirable to reduce processing power and implementation demands. The controllers were designed based on the linearised plant at the flight condition 20 kt but tested at the other flight conditions to ensure stability and desired performance.

The mixed-sensitivity design approach is well suited for vibration reduction applications because it consists of shaping two key closed-loop sensitivity transfer functions: $S(s) = (I - G(s)K(s))^{-1}$ and $K(s)S(s)$. The shaping takes place in the frequency domain. The sensitivity $S(s)$ is particularly important as it contains the information in terms of vibration reduction levels at steady-state, convergence rate and robustness. The shaping of $K(s)S(s)$ is included to account for the magnitude of the trailing edge flap deflection angles when performing the control task. The problem of shaping the above key transfer functions can be represented as finding a stabilizing controller $K(s)$ such that the following norm

$$\left\| \begin{bmatrix} W_p S \\ W_u K S \end{bmatrix} \right\|_\infty \tag{2}$$

is less than one of smaller[12]. The performance weight $W_p(s)$ and control efforts weight $W_u(s)$ are used to shape the sensitivity transfer function $S(s)$ and the control efforts $K(s)S(s)$, respectively. The standard choice of the performance weight is a 12-

by-12 transfer function matrix

$$W_p(s) = \begin{bmatrix} W_{p1}(s) & & \\ & \ddots & \\ & & W_{p12}(s) \end{bmatrix}$$

with diagonal elements as

$$W_{pi}(s) = \frac{s/M_i + \omega_{B_i}}{s + \omega_{B_i} A_i} \quad i = 1,.,12$$

The parameters M_i, ω_{B_i} and A_i were chosen to specify robustness, closed-loop bandwidth and steady-state performance levels, respectively. The control signal weight $W_u(s)$ is used to shape the control efforts $K(s)S(s)$ and it was chosen as a constant diagonal 2-by-2 matrix. After running the $\mathscr{H}_\infty$ optimisation algorithms in Matlab's Control System toolbox, the resulting controller is a transfer function matrix of very high order (order 90), due to the high dimensions of the open-loop problem. These limitations could be overcome by using model order reduction techniques without the robustness and performance being too compromised.

4.1. Linear Design Results

This subsection provides a brief presentation and a preliminary assessment of the results achieved with the obtained controller when performing on the linear approximation. As shown in Figure 13, the design objectives specified by performance and control efforts weights are largely satisfied because the peak values of the sensitivity transfer functions are less than the largest singular value of the performance weight reciprocal $W_p(s)^{-1}$ (dashed line) for a large number of frequencies. The design results are thus satisfactory in the sense that it provides closed-loop stability and can achieve reduction across all output channels for some directions of the baseline vibration.

The average vibration reduction of the output channels for linear simulation is about 80% as shown in Figure 14 and largest settling time around 23 s as shown in Figure 15. Control actions are also well within the actuator tolerance as shown in Figure 16.

4.2. Nonlinear Results

The performance of the controller was very similar to the results obtained with the linear approximation of the rotor behaviour. The convergence times were very similar, with the largest settling time around 23 s and the transient responses of the hub load coefficients showing no overshoots.

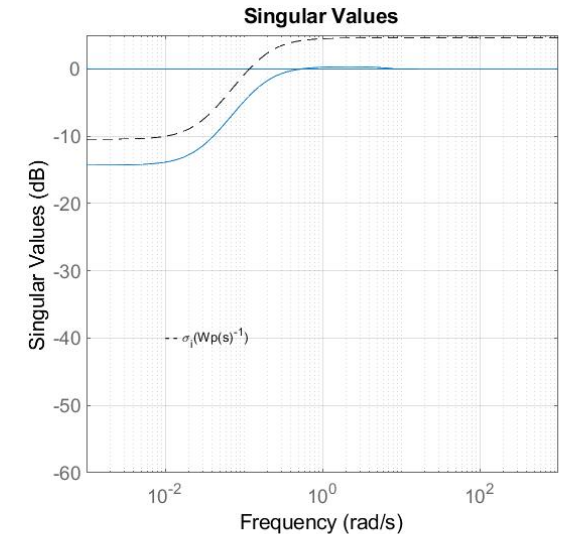

Figure 13: Sensitivity S and weighting performance W_p

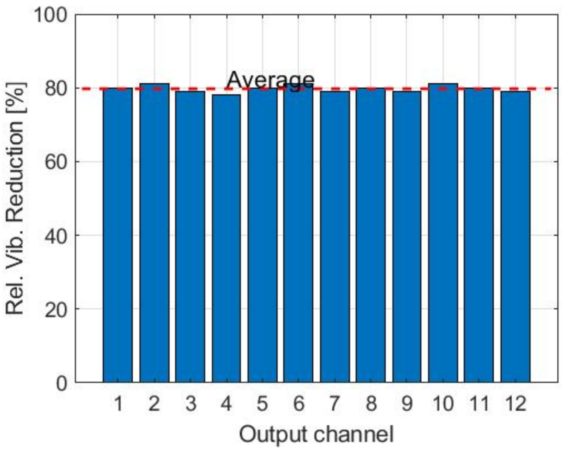

Figure 14: The average vibration reduction of the output channels for linear simulation

Steady-state vibration reduction levels in the desired channels are obtained by more than 68% in average, as shown from Figures 17 to Figures 22. The performance is deemed as highly satisfactory in the sense that simultaneous vibration reduction was achieved on all coefficients with significant vibration reduction and one controller operating for all flight conditions. We proceed next to assess the stability and performance robustness characteristics of the control system based on the linear approximation of the rotor behaviour.

4.3. Stability and Performance Characteristics

Another advantage of obtaining an LTI approximation of the rotor behaviour is that metrics for the

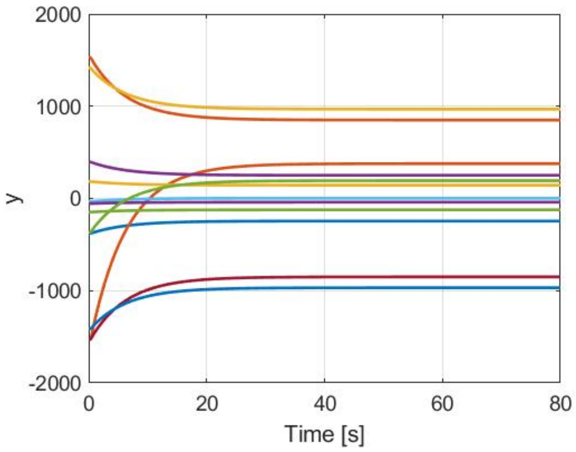

Figure 15: Output responses under linear simulation

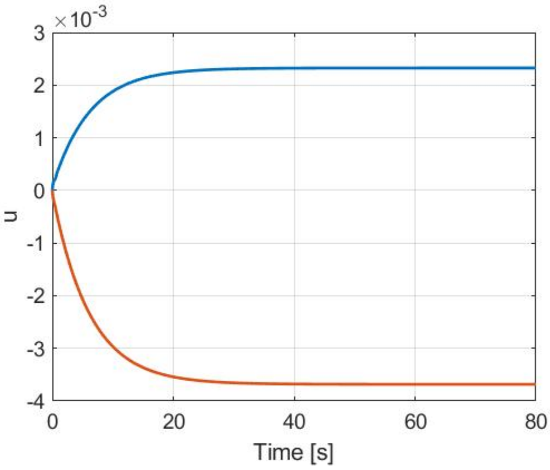

Figure 16: Control actions response

stability and performance robustness of the OBC system can be obtained. This is particular useful in practical applications to gain a higher confidence in the reliability of the OBC system. By stability robustness we refer to the property that stable operation in guaranteed in the presence of changes in the frequency characteristics of the rotor vibration behaviour, which in this case is due to operation for a wide number of flight conditions. On the other hand, performance robustness ensures that the single designed controller satisfies the performance design requirements across the considered flight envelope.

We first check *nominal* stability with the nominal behaviour considered at 20 kt. Nominal stability is satisfied, this is tested by ensuring that all the poles of the sensitivity transfer function $S(s)$ have negative real part, as shown in Figure 23. The condition to check if the performance is satisfied for the nominal flight condition is simply tested by the following

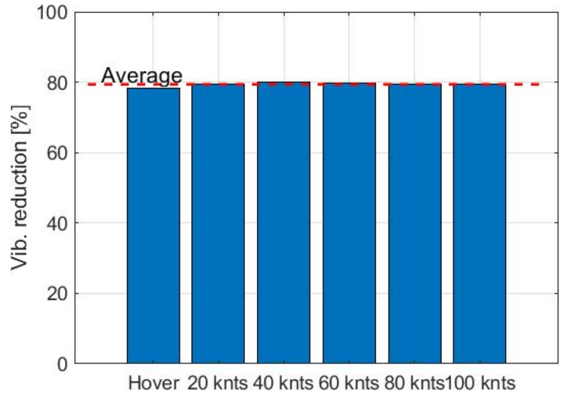

Figure 17: Nonlinear vibration reduction of the rotor thrust

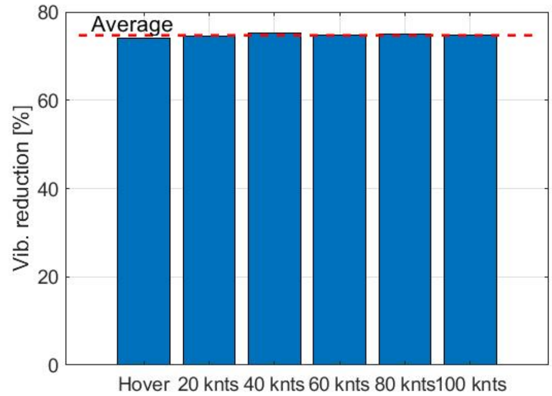

Figure 18: Nonlinear vibration reduction for H

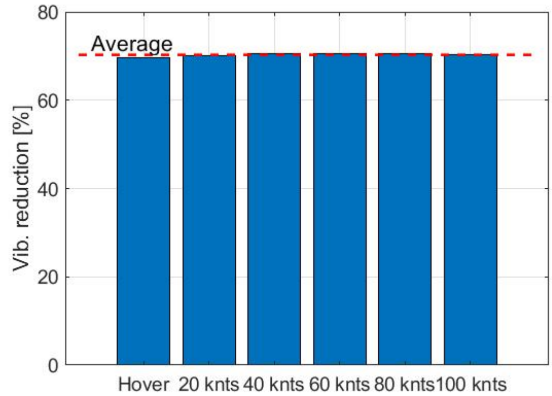

Figure 19: Nonlinear vibration reduction for Y

condition

$$\|W_p S\|_\infty = 0.8031 < 1$$

For testing *robust* stability, we model variations in the vibration open-loop behaviour with a standard

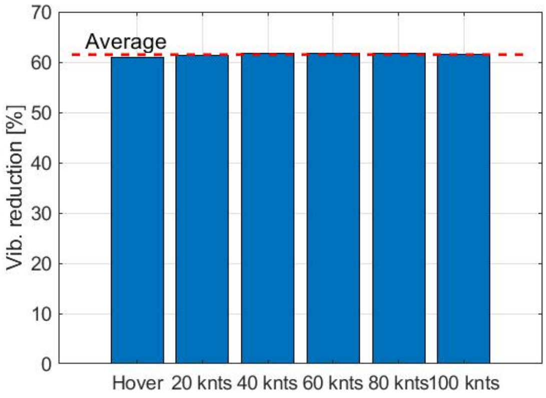

Figure 20: Nonlinear vibration reduction for M_x

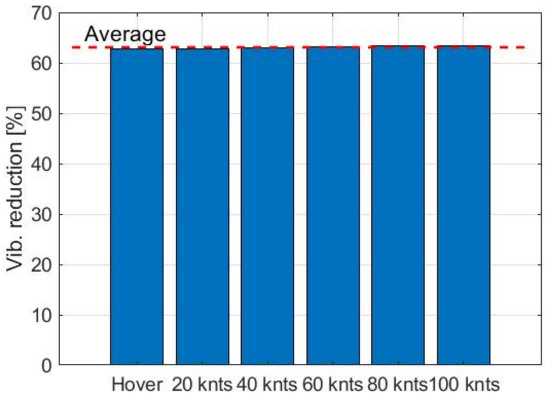

Figure 21: Nonlinear vibration reduction for M_y

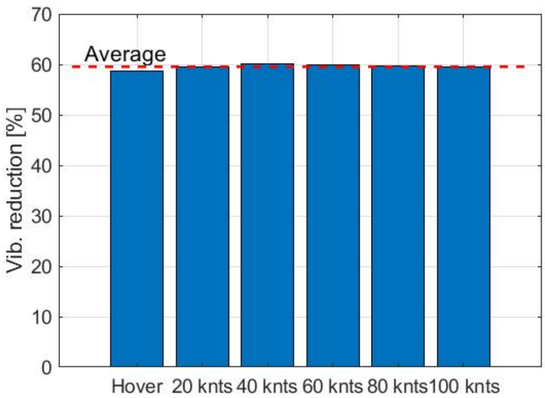

Figure 22: Nonlinear vibration reduction for Mz

multiplicative uncertainty model[12]. Control theory establishes that the feedback control system is robustly stable if

$$\|W_I T\|_\infty = 0.0891 < 1$$

So for the present case, the closed-loop system is

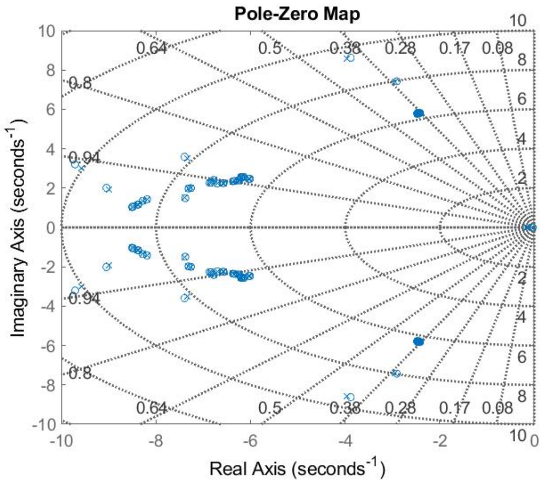

Figure 23: Poles of the sensitivity transfer functions $S(s)$

indeed robust stable. In the above condition $W_I(s)$ is a transfer function matrix required to model the uncertainty in the open-loop behaviour. Finally, the condition used to check *robust* performance is

$$\|W_p S + W_I T\|_\infty = 0.8148 < 1$$

which in this case the designed controller ensures that under the LTI approximation, the controller satisfies the vibration reduction performance requirements across the flight envelope.

5. COMPARISON BETWEEN CONTROLLERS

The purpose of this section is to compare the results obtained with the comprehensive controller described in this manuscript and the control approach by Alotaibi and Morales[2]. In this alternative approach, the authors achieve vibration by controlling only the thrust 4/rev components. For a more realistic comparison, the two controllers were implemented in discrete-time form with a sampling time equivalent to the time it takes for the blade to advance one-degree azimuth angle; no effects on performance and stability were registered due to this discretisation.

As seen from the simulation results by both control schemes, the design and implementation of both controllers are deemed satisfactory in terms of the performance achieved. The performance in both vibration reduction controllers is broadly similar in terms of steady-state vibration reduction ratios and convergence times, while a comprehensive controller provides smoother convergence but at a higher implementation cost. Both controllers are able to stabilise the system and reach the steady-

Hub Loads	Av. Vib. red. K_1 [%]	Av. Vib. red. K_2 [%]	Diff. [%]
T	72	79.4	7.4
H	39.8	74.7	34.9
Y	40	70.3	30.3
M_x	37.9	61.5	23.6
M_y	38.9	63.1	24.2
M_z	54	59.5	5.5
Average	55.6	68.1	21

Table 1: Percentage of the vibration reduction

state within 23 seconds.

We compare the average vibration reduction (Av. Vib. Red.) at 4/rev frequency component for all output channels and across the flight envelope, as shown in Table 1. The comprehensive controller (denoted as K_2) performs better in terms of vibration reduction for all hub loads and across the considered flight envelope. The vibration reduction is improved for all output channels by 21% in average, in comparison to the simpler controller approach (K_1) pursued by Alotaibi and Morales in 2018[2]. The simpler controller achieves an average of about 55.6% vibration reduction while the comprehensive controller offers an average of about 68.1 %. In particular, the comprehensive approach offer most improvements in reducing 4/rev rotor drag components, while the improvements on the 4/rev thrust and torque around the shaft components are minor, at less than 10%.

Note also that although the simpler approach only control the thrust component, this method does not lead to an increase in the other hub loads. This is a particular attractive feature of this method since it reduces significantly the implementation requirements of this controller. The simple controller is a 16th order transfer function matrix running at a reasonably large sampling time, making its implementation very appealing in real applications. On the other hand, the comprehensive controller requires noticeably more computational power, making perhaps difficult in real applications. The considered comprehensive controller is very high-order but this issue could be overcome by order-reduction methods[12].

Both controllers exploit the LTI dynamic representation of the thrust vibration harmonics to deploy a single controller which can operate over a wide region of the flight envelope. This is a desired property in practical implementations because it could avoid potential stability issues encountered by gain-scheduling-type or controller-switching approaches in addition to savings in memory. Linear representations of the open-loop vibration behaviour make it possible to obtain robustness and develop measures of the stability properties for both controllers around a specific operating condition.

6. FINAL REMARKS

We have discussed in this manuscript a comprehensive approach to achieve simultaneous vibration reduction on all rotor hub loads by a single control law operating over a wide range of the flight envelope. The method described here was shown to be highly satisfactory because of the vibration reduction level achieved, convergence times, control efforts and robustness properties. The method however requires high computational demands, which can be alleviated by the use of order-reduction methods or direct control of the rotor thrust 4/rev components only[2]. The comprehensive approach was shown to offer most improvements in reducing 4/rev rotor drag components, while the improvements on the 4/rev thrust and torque around the shaft components are minor with respect to the simpler approach of controlling the rotor thrust only. This and previous studies suggests that $\mathscr{H}_\infty$ have a lot potential when implemented on OBC applications, dealing well with the high dimensionality of the vibration control problem and improved robustness properties. Future research compare these methods with more popular methods such as those based on on-line optimisation laws[3] and Principal Components[4,14,13].

REFERENCES

[1] J. Alotaibi and R. M. Morales. Efficient implementation of a helicopter hingless rotor model with active trailing edge flaps for control design. In *Proceedings of the 12th UKACC Conference*, pages 93–98, 2018.

[2] J. Alotaibi and R. M. Morales. Mixed-sensitivity $\mathscr{H}_\infty$ on-blade control. In *Proceedings of the 44th European Rotorcraft Forum*, 2018.

[3] S. Boyd and L. Vandenberghe. *Convex Optimization*. Cambridge university press, 2004.

[4] S. J. Elliott. *Signal Processing for Active Control*. Academic Press, 2001.

[5] F. H. Fan and S. R. Hall. An $\mathscr{H}_\infty$ technique for improved higher harmonic control. *Proceedings of the 68th AHS Annual Forum*, 2012.

[6] P. P. Friedmann. On-blade control of rotor vibration, noise and performance: Just around

the corner? *Journal of the American Helicopter Society*, 59:(1–37), 2014.

[7] W. Johnson. Self-tuning regulators for multicyclic control of helicopter vibration. Technical Report NASA TP-1996, NASA, 1982.

[8] W. Johnson. *Rotorcraft Aeromechanics*. Cambridge University Press, 2013.

[9] C. Kessler. Active rotor control for helicopters: motivation and survey on higher harmonic control. *CEAS Aeronautical Journal*, 1(1-4):23–54, 2011.

[10] J.-B. Maurice, F. A. King, and W. Fitcher. Derivation and validation of a helicopter rotor model with trailing-edge flaps. *Journal of Guidance, Control, and Dynamics*, 36(5):1375–1387, 2013.

[11] J. Shaw and N. Albion. Active control of the helicopter rotor for vibration reduction. *Journal of the American Helicopter Society*, 26(3):32–39, 1981.

[12] S. Skogestad and I. Postlethwaite. *Multivariable Feedback Control: Analysis and Design (second edition)*. John Wiley & Sons, 2005.

[13] H. Yang, J. Alotaibi, and R. M. Morales. Advanced On-Blade Control for Vibration Reduction of the EC-145 Helicopter: Robust Principal Components vs $\mathscr{H}_\infty$. In *Proceedings of the AIAA Science and Technology Forum and Exposition*, Orlando, USA, 2020.

[14] H. Yang, R. M. Morales, and M. C. Turner. Robust principal component algorithms for high-order fast-sampled systems. In *Proceedings of the 17th European Control Conference*, Naples, Italy, 2019.